Analytical Methods

International Edition: DOI: 10.1002/anie.201600853
German Edition: DOI: 10.1002/ange.201600853

Individual Detection and Electrochemically Assisted Identification of Adsorbed Nanoparticles by Using Surface Plasmon Microscopy

*Shavkat Nizamov, Olga Kasian, and Vladimir M. Mirsky**

Abstract: *The increasing production and application of nanoparticles necessitates a highly sensitive analytical method for the quantification and identification of these potentially hazardous materials. We describe here an application of surface plasmon microscopy for the individual detection of each adsorbed nanoparticle and for visualization of its electrochemical conversion. Whereas the adsorption rate characterizes the number concentration of nanoparticles, the potential at which the adsorbed nanoparticles disappear during an anodic potential sweep characterizes the type of material. All the adsorbed nanoparticles are subjected to the potential sweep simultaneously; nevertheless, each of the up to a million adsorbed nanoparticles is identified individually by its electrochemical dissolution potential. The technique has been tested with silver and copper nanoparticles, but can be extended to many other electrochemically active nanomaterials.*

Numerous studies have demonstrated the toxicity of some engineered nanoparticles (NPs) for human health and the environment.[1–3] Therefore, analytical techniques for the ultrasensitive detection and identification of nanomaterials are highly desired. For this purpose, we suggest a new technology for counting, tracking, and electrochemically identifying each single NP by using highly sensitive surface plasmon microscopy (SPM) in combination with electrochemical treatment. SPM was originally developed as an imaging refractometry[4] to extend the performance of integral surface plasmon resonance (SPR) biosensors.[5] Recently, it was reported that the adsorption of single NPs to a SPM sensor surface leads to characteristic images[6–10] that are well-described by electrodynamic models.[11] However, these images, being dependent on the size, shape, and complex refractive index, can be very similar for NPs of different materials. To make a chemical identification of NPs we have complemented the real-time counting of each NP adsorbed on the SPM sensor with the detection of changes in its SPM image during electrochemical treatment. This individual electrochemical analysis of NPs is performed using an optical readout, thus avoiding many limitations of impact electrochemistry[12,13] or integral electrochemical techniques.[14] The Kretschmann configuration of SPM (Figure 1) allows us to use the advantages of a macroscopic sensor surface area and to perform simultaneous tracking of up to a million adsorbed nanoparticles.

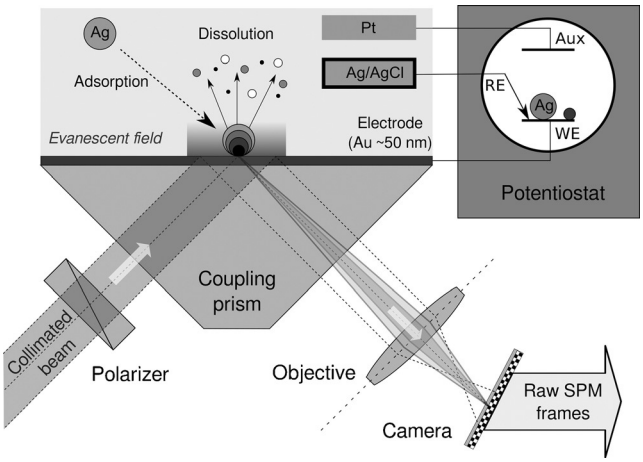

Figure 1. Surface plasmon microscopy setup for detecting, tracking, and in situ electrochemical treatment of adsorbed nanoparticles. The gold layer in the set-up has two functions: a plasmonic sensing surface and a working electrode that controls the redox state of the adsorbed NPs.

The method consists of three steps (Figure 2). The first one comprises an adsorption of NPs to the sensor surface at a cathodic potential, detection and counting of these NPs, and determination of the adsorption rate. During the washing step, unadsorbed NPs are eluted from the measurement cell. Finally, the electrical potential of the gold electrode (SPM sensor surface) is scanned in the anodic direction, and a disappearance of the adsorbed NPs is detected. The value of the electrode potential at which these NPs dissolve and disappear provides information on their chemical composition.

The adsorption of a single NP to the sensor surface is revealed by a change in the SPM images in a localized group of pixels. The changes are small but become highly visible after a preprocessing, which includes averaging the original image frames for about one second (Figure 2, first row) and calculating differential frames (second row). After the preprocessing, the nth differential frame is a pixel-to-pixel ratio of the $(n+1)$ averaged frame to the $(n-1)$ one. Such dynamic referencing suppresses a slow drift of the background of the SPM images and provides a much higher signal-to-noise ratio of the output signal than the referencing of each frame to the first (or to any other arbitrarily chosen) frame.

Injection of a suspension of NPs into the flow cell leads to a "rain" of such clearly visible characteristic images in the sequence of differential frames. As a consequence of the

[*] Dr. S. Nizamov, Dr. O. Kasian, Prof. Dr. V. M. Mirsky
Department of Nanobiotechnology, Institute of Biotechnology
Brandenburgische Technische Universität Cottbus—Senftenberg
01968 Senftenberg (Germany)
E-mail: mirsky@b-tu.de

Supporting information for this article can be found under: http://dx.doi.org/10.1002/anie.201600853.

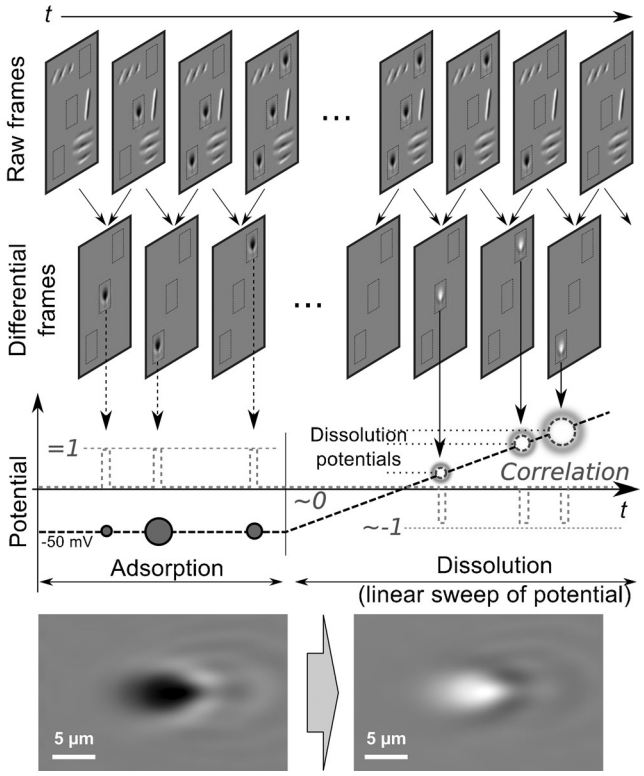

Figure 2. Determination of the dissolution potential of single nanoparticles using differential surface plasmon microscopy. The adsorption and dissolution of nanoparticles in differential frames are revealed by "positive" and "negative" images of the nanoparticle (bottom, for 60 nm Ag NPs).

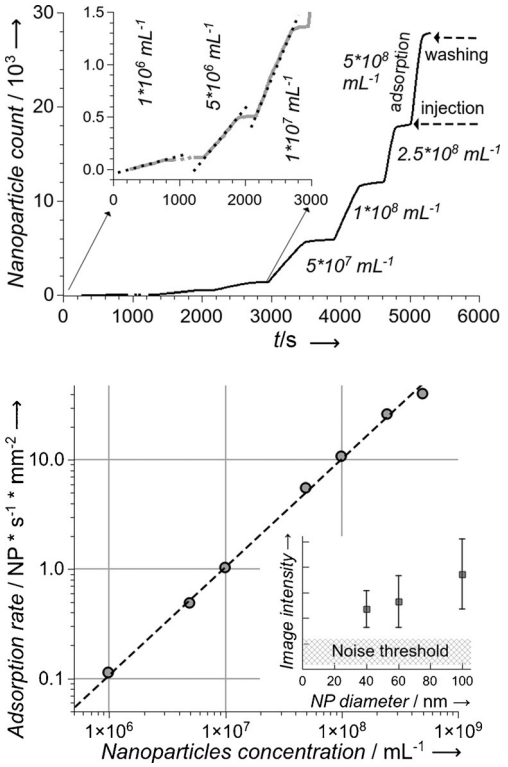

Figure 3. Adsorption kinetics for 60 nm Ag NPs during subsequent injections of their suspensions with different concentrations (top) and corresponding concentration dependence of the adsorption rate (bottom). Inset, bottom: Dependence of the maximal signal intensity on the size of the Ag NPs. Note that the number of adsorbed nanoparticles was determined by detecting and counting each single NP.

dynamic referencing, these images appear only in 2 or 3 consecutive differential frames, but can be spread to 1 or 2 frames more as a result of the averaging. A typical differential image of the adsorbed NP is shown in Figure 2 (bottom left). This is close to the theoretical prediction,[11] but, because of the limitations in optical resolution, a single particle that is smaller than the wavelength leads to an image with a typical size of $5 \times 10\ \mu m^2$.

The position of each NP adsorbed on the sensor surface was determined and saved. The adsorption rate was determined by counting the number of single NPs in each differential frame. The number of detected Ag NPs for the sequential injection of suspensions of 60 nm Ag NPs with different NP concentrations is shown in Figure 3. To prevent spontaneous oxidation of Ag NPs, the experiment was performed at a cathodic potential. Injections of NPs were performed during 100–1000 s (longer times for lower concentrations), followed by washing for 200 s. As expected for the fixed diffusion conditions (constant flow rate and viscosity of the electrolyte), the adsorption rate is proportional to the concentration of the NPs in the whole studied concentration range (10^6–10^9 NPs mL^{-1}; Figure 3, bottom). This dependence can be used for the analytical determination of NP concentrations.

Taking into account that the surface coverage is less than 1% even with a million NPs on a 1 mm^2 sensor surface, a possible influence of surface coverage on adsorption can be neglected. At a concentration of 1×10^6 NPs mL^{-1}, the adsorption rate per 1 mm^2 is about one NP per 10 s. This defines the detection limit of our method: if the detection of one NP during a reasonable measurement time of about 1000 s is sufficient, the limit of detection is approximately 10^4 NPs mL^{-1}. Further improvement of the detection limit can be achieved by increasing the sensor area, optimization of diffusion conditions, or by active collection of NPs near the sensor surface (i.e. by electrophoresis).[15]

The suggested analytical technique requires chemical conditions leading to the formation of soluble products after electrochemical oxidation of the NPs. Usually, complexing agents are used.[16] Electrochemical dissolution of Cu and Ag can be performed in electrolytes containing SCN^-, Cl^-, or CN^- at high concentrations to generate charged complex ions (e.g. $AgCl_2^-$) instead of neutral insoluble salts. The rate of electrochemical degradation of a gold electrode in the presence of chloride ions is much lower than in the presence of SCN^- or CN^-;[16] therefore, a chloride-containing electrolyte was chosen for the present study. The dependence of the peak potential of the oxidation of Ag NPs in the anodic voltammogram on the sweep rate corresponds to the irreversible one-electron transfer (Supporting Information Figure S1 a,b) with a charge transfer coefficient of 0.41 (Supporting Information Figure S2). The diffusion coefficient of Ag

NPs, determined from the slope of the dependence of the peak current on the square root of the potential sweep rate (Supporting Information Figure S3), is $1.4 \times 10^{-11}\ m^2 s^{-1}$ and corresponds to a hydrodynamic diameter of about 31 nm. This is close to the value of 37 nm obtained by dynamic light scattering (DLS) measurements (Supporting Information Figure S4). The voltammogramm of the electrochemical oxidation of Cu NPs shows a single peak, whose potential is independent of the sweep rate. This indicates that the oxidation occurs as a reversible two-electron transfer (Supporting Information Figure S5). The diffusion coefficient, calculated from the slope of the dependence of the peak current on the square root of the potential sweep rate, is $5.8 \times 10^{-12}\ m^2 s^{-1}$ (Supporting Information Figure S6) and corresponds to the Cu NPs having a hydrodynamic diameter of about 75 nm. This is close to the value of 80 nm obtained by DLS measurements (Supporting Information Figure S7).

One can expect that the appearance of a nanoparticle on the sensor surface (through adsorption) and its further disappearance (through desorption or electrochemical dissolution) will lead to the differential SPM images having the same shape and intensity but of opposing signs (e.g. Figure 2, bottom, left and right). This implies that the regression coefficient (RC) or normalized correlation coefficient between two images of the same NP (corresponding to its appearance and disappearance) are close to −1. The RC is more informative than the normalized correlation coefficient (see the Supporting Information) for quantitative analysis of gradual changes. The disappearance events occur very rarely at cathodic potentials: once per several hundreds of adsorption events. Therefore, the adsorption of metallic NPs under such conditions is practically irreversible. However, if the electrode potential is scanned in the anodic direction, the disappearance events of adsorbed NPs occur very frequently. This is certainly caused by electrochemical oxidation of the NPs and their dissolution.

The exemplary sequence of differential SPM images, corresponding to the adsorption and electrochemical dissolution of the same single Ag NP, is shown in Figure 4. An adsorption of this NP leads to the appearance of a dark spot (top left). As a consequence of dynamic referencing, this spot becomes invisible in the subsequent differential frames. When the electrode potential reaches the value required for electrochemical dissolution of this nanoparticle, an image with inverse intensity appears in the same place (bottom left). The kinetics of the regression coefficient of the image at the position where this NP was adsorbed, is shown in Figure 4 (right). Most of the time, the RC fluctuates around zero, thus indicating no changes in the NP state. The positive spike corresponds to the adsorption event (by definition, in this case RC = 1), and the negative spike corresponds to the disappearance of the NP. Thus, the electrode potential at which a NP dissolves, and which is characteristic of its content and size, can be determined simultaneously for each adsorbed NP.

The results of such an analysis for sequential measurements of 40, 60, and 100 nm Ag NPs, as well as for 50 nm Cu NPs, are shown in Figure 5, top. At the beginning of the potential sweep, the value of RC for all the detected NPs fluctuates around zero, thereby indicating that no appearance/disappearance events occur. However, at some defined value of the electrode potential, a strong shift of the RC in the negative direction is observed. This means that the images with inverse intensity to their values during the adsorption of NPs are detected in the groups of pixels corresponding to the positions of the adsorbed NPs. This indicates clearly a disappearance of the NPs from the surface. The fact that this process occurs only if some defined value of the electrode potential is reached indicates that the disappearance of the NPs is caused by their electrochemical dissolution. For Ag NPs, the size detection limit of our SPM setup is about 20 nm. Therefore, the observed disappearance of Ag NPs indicates that their size decreases below this value. For thermodynamic reasons, once an NP starts dissolving and shrinking in size at some particular potential, this process should continue until the dissolution of the NP is complete or there is a loss of its electrical contact to the electrode. Complete electrochemical dissolution of Ag NPs has already been reported.[13]

The expected difference between dissolution potentials of Ag and Cu NPs is clearly visible (Figure 5). The exact potentials vary for different NPs of the same nominal size and material. The reasons could be size variations, impurities, electrical barriers between the NPs and electrode surface (e.g. through surfactants), or local differences in the crystal planes of the gold electrode. The dissolution potential decreases as the size of the NP decreases (Figure 5); such an effect was analyzed thermodynamically[17,18] and confirmed by electrochemical experiments.[19–21] However, because of essential quantitative discrepancies in the observed values of the dissolution potential of NPs reported in the literature[21–24] and the broad distribution of this value for some types of NPs (Figure 4), it may be more reliable to determine the size of the NPs from the image intensity, not from the potential shift

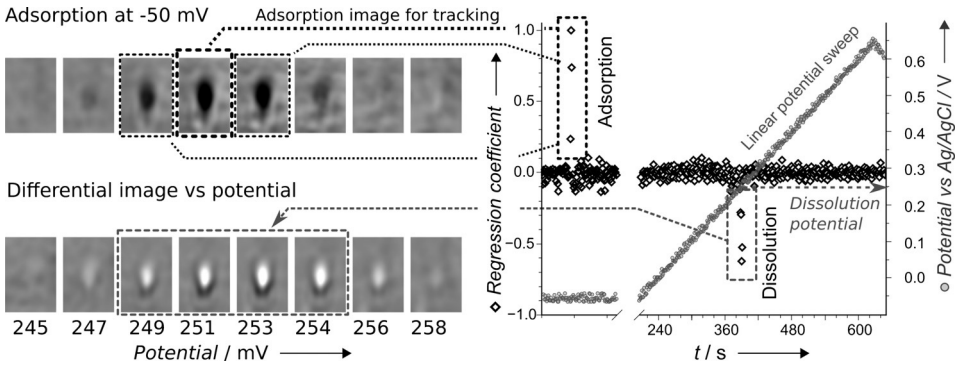

Figure 4. Determination of the dissolution potential of a single nanoparticle using differential SPM. Differential images corresponding to adsorption (top left) and dissolution (bottom left) of the same NP, and corresponding changes in the regression coefficient (right).

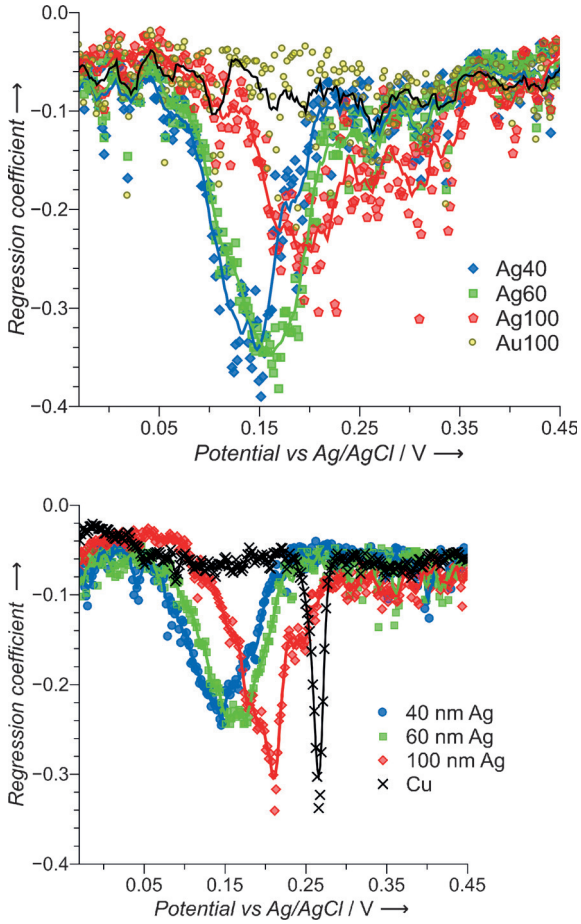

Figure 5. Regression coefficient for different types of nanoparticles versus the applied potential sweep. Top: Separate analysis for each NP type. Bottom: Sequential adsorption but simultaneous analysis within a single potential sweep of 1.5 $mV s^{-1}$.

(Figure 3, bottom, inset). The main goal of electrochemical analysis in this case is the chemical identification of the material of the NPs from the characteristic range of dissolution potentials. Notably, the characteristic potentials of the electrochemical dissolution in our case were determined for each individual NP and without electrochemical measurements.

A simultaneous analysis of different NPs is also possible (Figure 5, bottom). Thus, 40, 60, and 100 nm Ag NPs and 100 nm Au NPs were adsorbed sequentially on the sensor surface at a cathodic potential (−50 mV versus Ag/AgCl). The RCs for each adsorbed NP were determined during a single potential sweep in the anodic direction. Au NPs, used as a negative control, do not display any potential peak for dissolution. The peaks of the RC for Ag NPs of different size are observed at the same potentials as if each size was measured individually.

SPM detection and measurement of the concentration of NPs can be performed not only in pure laboratory samples but also in much more complex probes such as tap or mineral water, sunscreen cream, juice, or wine.[25] To determine the material of the NPs requires combination with a technique for material analysis. Herein, we have demonstrated an individual material analysis of each adsorbed Cu and Ag NP. The analysis is based on the determination of changes in SPM images caused by controlled electrochemical dissolution of the NPs. The method might be applied to other types of electrochemical conversions that result in notable changes in the complex refractive index of NPs. The potential window of the method could be increased by using non-aqueous electrolytes. This provides a way for extending this technique to oxide NPs or NPs made from various organic redox-active materials.

Experimental Section

Citrate-stabilized Ag NPs were obtained from Sigma Aldrich. Powdered 50 nm Cu NPs were obtained from QuantumSphere. Prior to measurements, all the samples were characterized using DLS. The set-up for SPM was based on the Kretschmann configuration and optimized for $\lambda = 642$ nm and a SF-10 prism ($n = 1.72$) with a ca. 47 nm thick gold layer and 3 nm Ti sublayer. The RC in Figure 5 is shown at the level of the 5th percentile of all NPs. Other experimental details are described in the Supporting Information.

Acknowledgements

The work was partially supported by the FP7 EC Project "Nanodetector" (no. 280478). We are grateful to Profs. J. Ramsden and R. G. Compton for helpful comments and fruitful discussions. The assistance of Dr. K. Tonder and V. Scherbahn is acknowledged.

Keywords: analytical methods · electrochemical dissolution · electrochemistry · nanoparticles · surface plasmon resonance

How to cite: *Angew. Chem. Int. Ed.* **2016**, *55*, 7247–7251
Angew. Chem. **2016**, *128*, 7363–7367

[1] A. D. Maynard, R. J. Aitken, T. Butz, V. Colvin, K. Donaldson, G. Oberdorster, et al., *Nature* **2006**, *444*, 267–269.
[2] N. O'Brien, E. J. Cummins, *J. Environ. Sci. Health Part A* **2010**, *45*, 992–1007.
[3] A. B. Stefaniak, V. A. Hackley, G. Roebben, K. Ehara, S. Hankin, M. T. Postek, I. Lynch, W.-E. Fu, T. P. J. Linsinger, A. F. Thunemann, *Nanotoxicology* **2013**, *7*, 1325–1337.
[4] B. Rothenhäuesler, W. Knoll, *Nature* **1988**, *332*, 615–617.
[5] J. Homola, *Chem. Rev.* **2008**, *108*, 462–493.
[6] B. Huang, F. Yu, R. N. Zare, *Anal. Chem.* **2007**, *79*, 2979–2983.
[7] X. Shan, I. Díez-Pérez, L. Wang, P. Wiktor, Y. Gu, L. Zhang, W. Wang, et al., *Nat. Nanotechnol.* **2012**, *7*, 668–672.
[8] A. R. Halpern, J. B. Wood, Y. Wang, R. M. Corn, *ACS Nano* **2014**, *8*, 1022–1030.
[9] Y. Fang, W. Wang, X. Wo, Y. Luo, S. Yin, Y. Wang, et al., *J. Am. Chem. Soc.* **2014**, *136*, 12584–12587.
[10] A. Zybin, Y. A. Kuritsyn, E. L. Gurevich, V. V. Temchura, K. Überla, K. Niemax, *Plasmonics* **2010**, *5*, 31–35.
[11] A. Demetriadou, A. A. Kornyshev, *New J. Phys.* **2015**, *17*, 013041.
[12] E. J. E. Stuart, Y. G. Zhou, N. V. Rees, R. G. Compton, *RSC Adv.* **2012**, *2*, 6879–6884.
[13] Y. G. Zhou, N. V. Rees, R. G. Compton, *Angew. Chem. Int. Ed.* **2011**, *50*, 4219–4221; *Angew. Chem.* **2011**, *123*, 4305–4307.
[14] S. Kraus-Ophir, J. Witt, G. Wittstock, D. Mandler, *Angew. Chem. Int. Ed.* **2014**, *53*, 294–298; *Angew. Chem.* **2014**, *126*, 300–304.

[15] I. Sidorenko, S. Nizamov, R. Hergenröder, A. Zybin, A. Kuzmichev, B. Kiwull, R. Niessner, V. M. Mirsky, *Microchim. Acta* **2016**, *183*, 101 – 109.
[16] M. Nicol, *J. Gold Bull.* **1980**, *13*, 46 – 55.
[17] W. J. Plieth, *J. Phys. Chem.* **1982**, *86*, 3166 – 3170.
[18] G. Horanyi, *J. Phys. Chem.* **1985**, *89*, 2967 – 2968.
[19] O. S. Ivanova, F. P. Zamborini, *J. Am. Chem. Soc.* **2010**, *132*, 70 – 72.
[20] Y. L. Mikhlin, E. A. Vishnyakova, A. S. Romanchenko, S. V. Saikova, et al., *Appl. Surf. Sci.* **2014**, *297*, 75 – 83.
[21] K. Z. Brainina, L. G. Galperin, T. Y. Kiryuhina, A. L. Galperin, N. Y. Stozhko, A. M. Murzakaev, O. R. Timoshenkova, *J. Solid State Electrochem.* **2012**, *16*, 2365 – 2372.
[22] S. E. Ward Jones, F. W. Campbell, R. Baron, L. Xiao, R. G. Compton, *J. Phys. Chem. C* **2008**, *112*, 17820 – 17827.
[23] K. H. Ng, H. Liu, R. M. Penner, *Langmuir* **2000**, *16*, 4016 – 4023.
[24] D. M. Kolb, G. E. Engelmann, J. C. Ziegler, *Angew. Chem. Int. Ed.* **2000**, *39*, 1123 – 1125; *Angew. Chem.* **2000**, *112*, 1166 – 1168.
[25] S. Nizamov, V. Scherbahn, V. M. Mirsky, **2016**, unpublished results.

Received: January 25, 2016
Revised: March 10, 2016
Published online: May 3, 2016

